A Target Field Approach to the Design of RF Phase-Gradient Coils

J. Bellec[1], C-Y. Liu[1], S. B. King[2], and C. P. Bidinosti[1,3]
[1]Physics and Astronomy, University of Manitoba, Winnipeg, Manitoba, Canada, [2]MR Technology, NRC Institute for Biodiagnostics, Winnipeg, Manitoba, Canada,
[3]Physics, University of Winnipeg, Winnipeg, Manitoba, Canada

INTRODUCTION: Conventional MRI utilizes a set of B_0 gradient coils to impose magnitude gradients onto the B_0 field. This induces a spatially varying phase in the transverse magnetization. However, there are complications attributed to the rapid switching of the B_0 gradient fields, such as induced eddy currents in nearby conductors (including the patient), nerve stimulation, mechanical vibrations, and loud acoustic noises. Transmit array spatial encoding (TRASE) [1] is a novel gradient-free imaging technique relying on Tx RF phase gradients expressed as $\mathbf{B_1} = |\mathbf{B_1}|\exp(i\varphi_1(\mathbf{r}))$, to spatially encode the transverse magnetization as $M_T = |M_0|\exp(i\varphi_1(\mathbf{r}))$, where $\varphi_1(\mathbf{r}) = 2\pi\mathbf{k}_1\cdot\mathbf{r}$. Ideal phase gradients have a uniform $|B_1|$ and strong-linear $\varphi_1(\mathbf{r})$ over a large volume. To optimize TRASE MRI, a target field method was investigated to improve phase gradient coils relative to previous designs [1].

APPROACH: The target field method was originally introduced for the design of cylindrical gradient coils [2], but has recently been used in RF coil design [3,4]. As an initial investigation, we are taking particular interest in Eq. (4) of Ref. [4]. From this equation, it follows that there is a direct relation between the Fourier components of the $\mathbf{B_1}$ field and Fourier components of the current distribution on a cylindrical shell. We have adopted these relations to determine the winding pattern on a cylindrical shell (oriented with the patient axis) that generates a target RF phase gradient field. The method is comprised of the following steps: (1) the Fourier components of the target field are determined; (2) the current distribution is constrained to a cylindrical shell and the Fourier components are calculated, which is subsequently used to obtain the actual current distribution; (3) a stream function approximation is implemented to determine discrete winding patterns of unit current.

In this technique, the RF phase gradient fields are modeled as $\mathbf{B}_1^{Gx_i} = A(l,z)\left(\cos((s/a)x_i)\hat{\mathbf{e}}_1 + \sin((s/a)x_i)\hat{\mathbf{e}}_2\right)$, where $\hat{\mathbf{e}}_1$ and $\hat{\mathbf{e}}_2$ are perpendicular to the B_0 field, s is the phase gradient strength, a is the coil radius, and x_i is the direction of the gradient. The function $A(l,z)$ is an apodization factor that rapidly sets the field to zero near $z=l$, restricting the coil length. It was modeled as $A(l,z)=(1+(z/l)^6)^{-1}$.

RESULTS/DISCUSSION: For a horizontal B_0 magnet, a G_z phase gradient coil for $s = \pi$ was obtained and is shown in Fig. 1(a). For a vertical B_0 magnet, the G_y phase gradient coil for $s = \pi/2$ is shown in Fig. 2(a). From simulated magnetic fields, the B_1 magnitude and phase for both coils were calculated. The magnitude plots are normalized to the central $|B_1|$ value, and display contours of 10% deviation from the central value. The contours in the phase plots correspond to 10° intervals, where the central contour is zero.

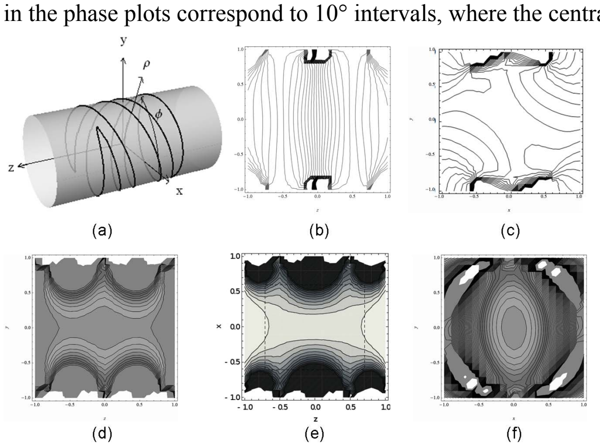

Fig. 1: Gz phase-gradient coil for horizontal B_0. (a) coil, (b) phase plot in sagittal plane, (c) phase plot in transverse plane, (d) magnitude plot in sagittal plane, (e) magnitude plot in coronal plane, (f) magnitude plot in axial plane.

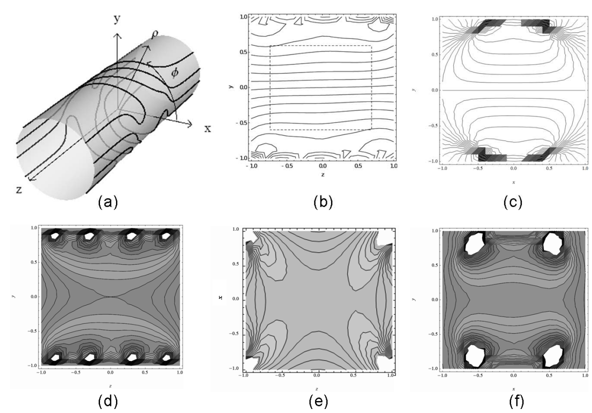

Fig. 2: Gy phase-gradient coil for vertical B_0. (a) coil, (b) phase plot in sagittal plane, (c) phase plot in axial plane, (d) magnitude plot in sagittal plane, (e) magnitude plot in coronal plane (f) magnitude plot in axial plane.

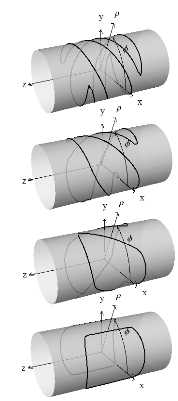

Fig. 3: Gz coils for s=π (top) to s=0 (bottom).

From Fig. 1(b) it appears that the phase is nearly linear in z, but from Fig. 1(c), the phase has some unwanted x and y dependencies. The $|B_1|$ homogeneity appears to vary as a function of the radial position ρ (Fig.1f), as well as with some off-axis z dependence (Fig.2d,e), and therefore has a limited region of homogeneity. Notice also that spiraling wire paths have a pitch that varies in z. These observations are consistent with spiral birdcages [5,6]. The phase distribution generated by the G_y phase gradient coil, in contrast to the G_z coil, is not only linear along the specified gradient axis (Fig.2b,c), but demonstrates almost no x or z dependence, as specified by the target field. However, the $|B_1|$ magnitude also has limited homogeneity (Fig.2c,d). Figure 3 shows that the G_z phase gradient coil starts as a saddle coil for $s = 0$, then becoming a saddle spiraling in z for larger s, resembling the spiral birdcage. Although an apodization factor was applied to the target field, it is unclear why the wires on the G_y phase gradient coil extend far beyond $z=\pm l$.

CONCLUSIONS: The target field approach has been used to determine current distributions that produce linear phase gradients and uniform magnitude, but over limited volumes. The fact that the horizontal-B_0 z-phase gradient design resembles initial spiral birdcage phase gradients, suggests that the approach is valid and deserves more attention. More work emphasizing uniform magnitude over a larger volume is needed to optimize the designs (including other gradient directions), but determining such complicated winding patterns may be difficult without a target field approach.

REFERENCES [1] JC Sharp and SB King, Magn Reson Med. 63:151-161(2010), [2] R Turner and RM Bowley, J Phys E **19**, 876 (1986). [3] Y Li et al, Conc. Magn Reson Part B: MR Eng., [4] CP Bidinosti *et al*., J Magn Reson **177**, 31 (2005). [5] SB King et al, Proc. ISMRM #4922 (2010), [6] CP Bidinosti et al, Proc. ISMRM #1509 (2010).